

Article

Radiological and Structural Characterization of Raw and Alkali-Activated Wood Ash and Metakaolin Blends

Nataša N. Mladenović Nikolić ^{1,*} , Aleksandar B. Kandić ¹ , Katarina V. Trivunac ², Miljana M. Mirković ³ , Ivana S. Vukanac ⁴, Snežana S. Nenadović ³  and Ljiljana M. Kljajević ³ 

¹ Department of Nuclear and Plasma Physics, “VINČA” Institute of Nuclear Sciences—National Institute of the Republic of the Serbia, University of Belgrade, 11000 Belgrade, Serbia

² Faculty of Technology and Metallurgy, University of Belgrade, 11000 Belgrade, Serbia

³ Department for Materials, “VINČA” Institute of Nuclear Sciences—National Institute of the Republic of the Serbia, University of Belgrade, 11000 Belgrade, Serbia

⁴ Department of Radiation and Environmental Protection, “VINČA” Institute of Nuclear Sciences—National Institute of the Republic of the Serbia, University of Belgrade, 11000 Belgrade, Serbia

* Correspondence: natasa.nikolic@vin.bg.ac.rs

Abstract: The aim of the presented research was to investigate the application possibility of wood ash and metakaolin to obtain alkali-activated materials as relatively new materials in the building industry. Thus, in order to assess the adequate use of these waste materials, structural and radiological characteristics should be considered. Until now, the focus has been on ash from thermal power plants produced by burning coal, but a large part of households in our country have individual fireplaces in which wood is used as the basic raw material; thus, it is very interesting to measure the activity concentration of radionuclide in wood ash as well as the possibility of reusing that ash for other purposes. All materials were studied, in terms of physical and chemical characteristics, by methods such as X-ray diffraction (XRD), Fourier transform infra-red (FTIR) spectroscopy, and scanning electron microscopy and energy-dispersive X-ray spectroscopy (SEM/EDS). XRD measurements of wood ash samples showed that it consists of calcite and larnite. FTIR spectroscopy revealed a polymeric Si–O–Al framework in alkali-activated materials and Si–O bonding bands corresponding to silicon dioxide. Determination of radionuclide content was performed by means of gamma-ray spectrometry. Results showed that the alkaline activation process led to the decrease in the activity concentration of radionuclides detected in the measured samples. External radiation hazard index (H_{ex}) for wood ash was reduced by more than 50% after alkali activation. The results of activity concentration measurements in alkali-activated materials indicate potential for their safe application in building construction.

Keywords: wood ash; metakaolin; alkali-activated materials; radionuclides



Citation: Mladenović Nikolić, N.N.; Kandić, A.B.; Trivunac, K.V.; Mirković, M.M.; Vukanac, I.S.; Nenadović, S.S.; Kljajević, L.M. Radiological and Structural Characterization of Raw and Alkali-Activated Wood Ash and Metakaolin Blends. *Sustainability* **2022**, *14*, 12960. <https://doi.org/10.3390/su142012960>

Academic Editor: Antonio Caggiano

Received: 14 September 2022

Accepted: 9 October 2022

Published: 11 October 2022

Publisher’s Note: MDPI stays neutral with regard to jurisdictional claims in published maps and institutional affiliations.



Copyright: © 2022 by the authors. Licensee MDPI, Basel, Switzerland. This article is an open access article distributed under the terms and conditions of the Creative Commons Attribution (CC BY) license (<https://creativecommons.org/licenses/by/4.0/>).

1. Introduction

Alkali-activated materials (AAM) can be used as alternative binders instead of Portland cement. They can be manufactured to have lower carbon dioxide emissions utilizing industrial and other residues. The main constituents of AAM are aluminosilicate precursors which are often waste-based materials. However, it is complicated to define the final AAM properties in their current state due to the diversity of material origins (metakaolin, fly ash, blast furnace slag, etc.). Therefore, every investigated system requires separate analysis depending on the aluminosilicate source materials that are used. AAM are formed by the reaction between an aluminosilicate precursor—such as metakaolin, different kinds of fly ashes, red clay brick waste, or concrete waste—and an alkaline activator. The mixture of sodium hydroxide (NaOH) and sodium silicate (Na₂SiO₃) or potassium hydroxide (KOH) and potassium silicate (K₂SiO₃) are usually used as an alkali activator [1–5]. The alkali

activation process of the precursors takes place at room temperature or curing at a temperature lower than 100 °C [2,6–8]. By alkaline activation, solid precursor raw materials are dissolved, and then polymerization of the dissolved species occurs. Polymeric chains are composed of tetrahedral silicate and aluminate units linked by covalent bonds in a three-dimensional structure. The negative charges associated with tetrahedral Al (III) are charge-balanced by alkali cations [9,10]. Metakaolin can be used as a main aluminosilicate precursor for AAM and also as a supplementary component in blended systems from which alkali-activated materials can be obtained. Good properties such as thermal, chemical, and mechanical can be the advantages of alkali-activated materials based on metakaolin [11,12]. In addition, metakaolin has a defected structure which leads to an increase in its reactivity [8]. The use of metakaolin for construction purposes provides technical and environmental benefits. Metakaolin is produced by heat treatment of kaolin clays in a certain temperature range. Heating parameters such as temperature, heating rate, and time, as well as cooling parameters during kaolin thermal treatment, affect the dehydroxylation process.

Wood and wood fuels, individually or combined with other fuels (wood/coal and combination wood fuels/other fuels), represent a dominant source of energy for heating households in Serbia [13]. There is no adequate legally prescribed disposal of the ash that is left behind after combustion, so it generally ends up in communal waste and is disposed of in municipal landfills. So far, a smaller percentage of wood ashes is used in agriculture, while very little is used for various other applications. Investigation of the liability of usage of wood ash as a partial cement substitution has been the subject of some studies [14–17]. By using ash as a partial and optional substitution for ordinary Portland cement, the utilization of natural raw materials and the quantity of disposed waste can be reduced [6,18,19]. Chemical composition of the wood ash depends on the type of wood and the working conditions of the combustion. According to Vassilev et al. [20], the content of CaO varies in the range of 5.79–83.46% depending on the type of wood and woody biomass [20,21]. The presence of calcium during the synthesis of AAM is significant since the ash could be hydraulically reactive [22,23]. However, some studies, such as Temuujin et al. [24], showed that product obtained by alkali activation of ashes rich with calcium does not improve the mechanical properties and durability, possibly due to sodium silicate precipitates as either calcium hydroxide or calcium silicate aluminate hydrate phases. The technology of alkali activation is gaining commercial interest because it has been demonstrated that, in certain cases, the properties of alkali-activated materials are superior to existing cementations systems [10].

Building materials can contain various amounts of naturally occurring radionuclides which contribute most to the population exposure through ionizing radiation. The external radiation hazard index, as well as radium equivalent activity, external absorbed gamma dose rate, and annual effective dose, can be determined based on measured activity concentration of natural radionuclides ^{226}Ra , ^{232}Th , and ^{40}K [25]. According to Temuujin et al. [24], the activity concentration of natural radionuclides after alkali-activation for two different ashes have values of 37.8 Bq/kg and 54.8 Bq/kg for ^{226}Ra , 15.6 Bq/kg and 17.2 Bq/kg for ^{232}Th , and 831.4 Bq/kg and 884.9 Bq/kg for ^{40}K , respectively. The interest in measuring radioactivity in terms of activity concentrations of selected and commonly present elements in building materials is due to its health hazards [25].

The aim of this paper is to assess the possibility of using wood ash in the production of alkaline-activated materials as cementations materials for potential application in the construction industry in order to find adequate reuse of waste material with regard to structural and radiological characteristics. The blended wood ash/metakaolin alkali-activated samples were prepared by the mixing of wood ash and metakaolin. The structural and radiological properties of obtained materials were used to assess the blended systems compared with a control sample containing 100% wood ash.

2. Materials and Methods

2.1. Synthesis of Alkali-Activated Materials

For the synthesis of AAM, calcined clay–metakaolin (MK), the wooden biomass ash (WA) from combustion process, and the blended samples WAMK were used as a precursor. Metakaolin was obtained by thermal treatment of the kaolin clay at 750 °C in an air atmosphere furnace, with heating rate 10° /min and soaking time at elevated temperature of one hour [26]. An alkaline activator was prepared by applying the procedure described in detail in Kljajevic et al. [27], by mixing of solution of 6M NaOH (Sigma-Aldrich, St. Louis, MO, USA) and Na₂SiO₃ solutions (Galenika Magmasil d.o.o, Belgrade, Serbia, technical grade). The content of Na₂O and SiO₂ was 12.3% and 22.5%, respectively. The volume ratio of solution of NaOH and sodium silicate solution was 1.5.

The mass share of MK in the mixed sample of MK and WA varied from 10% to 30%. Table 1 shows the mix design of WA and MK as the solid precursors of AAM. The ratio of liquid and solid phase was 0.8–1.0 depending on the processability of the mixture. Solid precursors and alkali activator were mixed for a very short time (maximum 5 min) and poured into molds, covered, and then left at room temperature for 24 h. Finally, the mixture was kept at 60 °C for an additional two days in appropriate covered molds. After drying in an oven, the samples were left at room temperature for 28 days in controlled conditions. Alkali-activated samples were prepared for characterization by crushing and sieved through a sieve with holes of size 355 µm. The obtained values (Table 2) represent the analysis of the elemental composition of raw materials, MK, and WA, performed using the XRF method (type UPA KSRF 200).

Table 1. Experimental design of WA and MK blends.

Samples	WA (%)	MK (%)
WA	100	0
WAMK10	90	10
WAMK20	80	20
WAMK30	70	30
MK	100	0

Table 2. Chemical composition of raw materials, WA and MK.

Chemical	SiO ₂	Al ₂ O ₃	Na ₂ O	CaO	K ₂ O	MgO	SO ₃	CuO	ZnO ₂	P ₂ O ₅	Mn ₂ O ₃	Fe ₂ O ₃	L.O.I.*
WA (wt.%)	3.40	/	2.35	66.2	13.4	2.28	0.95	3.60	4.31	1.10	1.82	/	0.59
MK (wt.%)	55.03	35.44	/	1.38	2.07	1.25	/	/	/	/	/	4.39	0.44

* Loss on ignition.

2.2. Experimental Techniques

2.2.1. Gamma Spectrometry

Activity concentration of naturally occurring radionuclides (uranium and thorium series, ⁴⁰K and ²³⁵U) and artificial radionuclide ¹³⁷Cs—in WA, MK, and a mixture of these materials, as well as in their alkali-activated forms—was determined by the semiconductor high purity germanium (HPGe) detector. Powdered samples were placed in PVC cylindrical containers (125 mL), sealed, and left for six weeks in order to reach radioactive equilibrium. Radiological analysis was performed by means of two coaxial spectrometers: AMETEK-ORTEC GEM 30-70, with 37% relative efficiency and 1.8 keV resolution at the 1332.5 keV line ⁶⁰Co; and Canberra GX5019, with 55% relative efficiency and 1.9 keV resolution at the 1332.5 keV line ⁶⁰Co. Certified solution of mixed gamma-emitting radionuclides (²⁴¹Am, ¹⁰⁹Cd, ¹³⁹Ce, ⁵⁷Co, ⁶⁰Co, ¹³⁷Cs, ¹¹³Sn, ⁸⁵Sr, ⁵¹Cr, ²¹⁰Pb, and ⁸⁸Y), purchased from the Czech Metrology Institute (CMI) [28], was used for the preparation of standards for the energy and efficiency calibration of the spectrometer in accordance with IAEA recommendations [29]. After reaching the radioactive equilibrium, samples were measured, and all spectra were recorded and analyzed using Canberra's Genie 2000 software; net areas of the peaks were

corrected for the background, dead time, and coincidence summing effects. All calculations were performed with the Mathematica 5.2 software (Wolfram Research, Inc., Champaign, IL, USA).

Activity concentration of ^{238}U was determined by using the evaluated activity of $^{234\text{m}}\text{Pa}$ (1001.0 keV), and the activity of ^{235}U was determined by analyzing net peak area at 143.729 keV. The activity of ^{226}Ra was determined via its decay products ^{214}Bi (609.31 keV, 1120.29 keV, and 1764.49 keV) and ^{214}Pb (295.22 keV and 351.93 keV), and additional testing was performed via 186.211 keV peak-corrected for ^{235}U (185.72 keV). The activity of ^{210}Pb was determined by analyzing its low energy peak at 46.54 keV. The activity of ^{232}Th was determined by using the evaluated activity of ^{228}Ac (338.34 keV, 911.20 keV, and 968.96 keV) and then via additional testing by other radionuclides from the thorium series, i.e., ^{212}Bi (727.33 keV), ^{212}Pb (238.63 keV), and ^{208}Tl (589.19 keV). The activity of ^{40}K was determined directly by analyzing net peak area at 1460.82 keV, subtracting the contribution of ^{228}Ac (1459.13 keV); the specific activity of ^{137}Cs was determined based on the line at 661.66 keV.

2.2.2. Assessment of Dosimetric Quantities

Radium equivalent activity (R_{eq}) is the index defined to obtain the sum of activities for comparison of specific radioactivity of materials containing different radionuclides ^{226}Ra , ^{232}Th , and ^{40}K , and it is defined as:

$$R_{eq} = A_{Ra} + 1.43A_{Th} + 0.077A_K$$

where A_{Ra} , A_{Th} , and A_K are activities in Bq/kg of ^{226}Ra , ^{232}Th , and ^{40}K , respectively [30,31].

We examine the characteristics of the material in order to assess the possibility of its use as a building material; for limiting the radiation dose from building material, the external hazard index (H_{ex}) is defined as [30]:

$$H_{ex} = \frac{A_{Ra}}{370} + \frac{A_{Th}}{259} + \frac{A_K}{4810} \leq 1$$

The value of this index must be less than unity to keep the radiation hazard insignificant, i.e., to keep the radium equivalent activity and annual dose under the permissible limits of 370 Bq/kg and 1 mSv, respectively [31].

The external absorbed gamma dose rate, \dot{D} (nGy/h), in air 1m above the ground due to radionuclides ^{226}Ra , ^{232}Th , and ^{40}K in measured samples was calculated [31]:

$$\dot{D} = 0.462A_{Ra} + 0.604A_{Th} + 0.0417A_K$$

In order to estimate the health risks, the annual effective dose rates was calculated using the conversion coefficient from the absorbed dose in air to the effective dose (0.7 Sv/Gy), the indoor occupancy factor (0.8)—assuming that people spend approximately 80% of the time indoors, and 8760 h (1 year) annual exposure time as proposed by UNSCEAR (1993). The annual effective dose (EDR) was calculated from the formula [32,33]:

$$EDR(\text{mSv}) = \dot{D}(\text{nGy/h}) \times 8760 \cdot (\text{h/y}) \times 0.8 \times 0.7 (\text{Sv/Gy}) 10^{-6}$$

2.2.3. Physico-Chemical Characterization

The functional groups of samples were studied using FTIR—Bomem (Hartmann & Braun, Frankfurt, Germany) MB-100 spectrometer. The spectral region of 400–4000 cm^{-1} was used for the determination of functional groups of investigated materials (wood ash, metakaolin, and their alkali-activated products). The mineralogy composition of raw materials and their alkali-activated products was determined by the XRD method using the Ultima IV Rigaku diffractometer (Rigaku, Tokyo, Japan) equipped with Cu $K\alpha_{1,2}$ radiation, with a generator voltage of 40.0 kV and a generator current 40.0 mA. The range of 5–80° 2θ was used for all powders in a continuous scan mode with a scanning step size of 0.02° at a scan rate of 5°/min. The PDXL2 software 2.8.4.0 (Rigaku, Tokyo, Japan) was used

to evaluate the phase composition and identification of all samples [34]. All obtained patterns were compared using the International Crystallographical Data base (ICDD) and the card numbers used to identify the phases were kaolinite: $\text{Al}_2(\text{Si}_2\text{O}_5)(\text{OH})_4$ -PDF No: 01-072-5860, muscovite: $\text{K}(\text{Al}_4\text{Si}_2\text{O}_9(\text{OH})_3)$ -PDF No: 01-070-375, quartz: SiO_2 -PDF No: 01-079-6237, illite: $\text{KAl}_2(\text{Si}_3\text{Al})\text{O}_{10}(\text{OH})_2$ -PDF No: 00-043-0685, calcite: CaCO_3 -PDF No: 01-071-3699, quartz: SiO_2 -PDF No: 01-079-6237, larnite: $\text{Ca}_2(\text{SiO}_4)$ -PDF No: 01-083-0464, illite: $\text{KAl}_2(\text{Si}_3\text{Al})\text{O}_{10}(\text{OH})_2$ -PDF No: 00-043-0685, and nepheline: NaAlSiO_4 -PDF No: 00-019-1176 [35]. The microstructure analysis was performed on a Au-coated surface of the samples using a Japan Electron Optics Laboratory electron microscope (JEOL JSM, Tokyo, Japan) 6390 LV at 25 kV coupled with energy dispersive X-ray spectroscopy (EDS), Oxford Instruments X-MaxN (Abingdon, UK).

3. Results and Discussion

3.1. Radiological Analysis

Activity concentration of naturally occurring radionuclides, as well as artificial radionuclide ^{137}Cs , in metakaolin, wood ash, and wood ash/metakaolin mixture are presented in Table 3. Table 4 shows the activity concentration of naturally occurring radionuclides and artificial radionuclide ^{137}Cs of synthesized AAM.

Table 3. Activity concentration (in Bq/kg) of gamma-emitting radionuclides in WA, MK, and mixture of WAMK.

	Activity Concentration [Bq/kg]				
	WA	WAMK10	WAMK20	WAMK30	MK
^{137}Cs	61.6 ± 3.2	38.0 ± 2.0	30.0 ± 1.6	27.1 ± 1.5	<0.1
^{210}Pb	53.5 ± 4.1	92.4 ± 5.5	117.2 ± 6.7	117.3 ± 7.0	119.7 ± 10.3
^{235}U	1.96 ± 0.40	3.06 ± 0.39	4.83 ± 0.88	4.62 ± 0.68	14.8 ± 1.3
^{226}Ra	35.3 ± 3.6	43.0 ± 4.4	69.4 ± 6.5	82.8 ± 6.5	209.6 ± 12.7
^{238}U	46.5 ± 6.0	55.0 ± 6.3	77.5 ± 7.6	81.8 ± 8.5	244.5 ± 11.9
^{234}Th (^{228}Ac)	34.0 ± 3.0	41.1 ± 3.0	47.7 ± 3.2	54.9 ± 3.7	105.4 ± 5.6
^{40}K	3840 ± 195	2840 ± 143	2475 ± 125	2268 ± 115	641 ± 33

Table 4. Activity concentration (in Bq/kg) of gamma-emitting radionuclides in alkali-activated GWA, GMK, and mixture of GWAMK.

	Activity Concentration [Bq/kg]				
	GWA	GWAMK10	GWAMK20	GWAMK30	GMK
^{137}Cs	22.1 ± 1.2	21.7 ± 1.1	18.2 ± 1.0	16.8 ± 0.9	<0.1
^{210}Pb	43.9 ± 3.4	51.3 ± 3.2	51.2 ± 3.0	58.2 ± 3.3	115.5 ± 5.7
^{235}U	0.68 ± 0.16	1.14 ± 0.28	1.55 ± 0.26	2.81 ± 0.51	9.35 ± 0.97
^{226}Ra	23.5 ± 2.8	35.1 ± 3.7	45.7 ± 4.0	54.4 ± 4.6	149.3 ± 9.1
^{238}U	28.1 ± 4.0	32.6 ± 3.2	50.1 ± 5.0	62.4 ± 6.4	161.1 ± 14.3
^{234}Th (^{228}Ac)	19.8 ± 1.5	27.6 ± 1.9	29.3 ± 2.0	34.3 ± 2.2	72.4 ± 3.9
^{40}K	1680 ± 80	1720 ± 90	1490 ± 70	1420 ± 70	455 ± 23

As can be seen from Tables 3 and 4, the values of measured specific activities are lower in alkali-activated samples. A possible explanation can be obtained by analyzing masses of non-activated materials during the synthesis process. Namely, the alkali-activation process requires the addition of a certain amount of solid materials (sodium hydroxide/sodium silicate) which would increase the mass of the sample, which could be the reason for specific activities decreasing in alkali-activated samples compared with raw materials. However, the addition of non-active constituents does not increase the mass of the samples significantly, so a complete explanation should be further pursued. A possible additional explanation could be a change in the physical properties of the samples (formation of a crystal lattice, etc.), which would affect the emission of ionizing radiation from the surface

of the samples. In addition, as the ratio of specific activities measured in raw materials and alkali-activated materials varies significantly for different radionuclides, the results obtained in these studies open new directions for further research.

The maximum value of ^{137}Cs activity concentration was in the sample of WA (61.6 ± 3.2 Bq/kg) and decreased with the increase of MK amount from 10% to 30%, which could be expected since this radionuclide was not detected in the MK sample, i.e., it was below minimal detectable activity—MDA (<0.1 Bq/kg). There were decreases in ^{137}Cs activity concentrations after alkali activation of all samples, but the most significant reduction was observed in the GWA sample from 61.6 ± 3.2 (WA sample) to 22.1 ± 1.2 Bq/kg (approximately 2.79 times).

Additionally, Ilić et al. [36] analyzed the clayey materials in Serbia, and they found that the activity concentration of ^{137}Cs was <0.1 Bq/kg, but the value for ^{40}K was in the range of 190–668 Bq/kg. Metakaolin, which was used in this work, also had <0.1 Bq/kg for ^{137}Cs , but for ^{40}K that value was 641 ± 33 Bq/kg; after alkali-activation the value decreased to 455 ± 23 Bq/kg [36].

According to Šešlak et al. [37], the radioactivity concentration of ^{137}Cs and ^{40}K in wood ash samples obtained by burning seven species of wood at different locations in Serbia were in the range of 1.2–1010 Bq/kg and 1160–4720 Bq/kg, respectively. In the raw material used in the presented research, the activity concentrations of ^{137}Cs and ^{40}K were 61.6 ± 3.2 Bq/kg and 3840 ± 195 Bq/kg, respectively. After the alkali activation process, those values were more than two times smaller.

It must be noted that ^{137}Cs presence is attributed mainly to the fallout of the Chernobyl accident. According to the investigation of Ladygienė et al. [38] of different wood samples, such as chips, briquettes, and pellets from different countries (Poland, Ukraine, Russia, and Belarus), the activity concentration of ^{137}Cs had a value from 21 ± 4 Bq/kg to 9800 ± 700 Bq/kg. In addition, research of Hus et al. showed that wood ash (ash from beech wood from Croatia) contained 194.6 Bq/kg ^{137}Cs , and it was within acceptable limits from the point of view of radiocontamination of the environment using wood as fuel [39]. The amount of radionuclides accumulated in plants can be one hundred times higher compared with radionuclide content in their habitat medium [40]. The ^{137}Cs concentrations of the wood ash samples from the Balkan area ranged from 31 Bq/kg to 64 Bq/kg, as well as 174 Bq/kg from pellets [41]. The activities measured in the ash samples were enriched with respect to the activities of the burned biomass products due to the removal of organic compounds during combustion. The “wood/ash” enrichment factor ranged from 107 to 118 for wood stoves, according to the results of Stoulos et al. The “wood/ash” enrichment factor was estimated using ^{40}K concentrations and assuming that K is not volatile and, thus, the potassium present in the raw material remains in the ash produced during the combustion [41].

R_{eq} , H_{ex} , \dot{D} , and EDR from MK, WA, and alkali-activated mixture of WAMK were determined and are presented in Tables 5 and 6.

Table 5. R_{eq} , H_{ex} , \dot{D} , and EDR of MK, WA, and mixture of WAMK.

Samples	R_{eq} (Bq/kg)	H_{ex} (Bq/kg)	\dot{D} (nGy/h)	EDR (mSv/y)
WA	379.6	1.025	197.0	0.966
WAMK10	320.5	0.865	163.1	0.800
WAMK20	328.2	0.886	164.1	0.805
WAMK30	335.9	0.907	166.0	0.814
MK	409.7	1.107	187.2	0.918

Table 6. Ra_{eq} , H_{ex} , \dot{D} , and EDR of alkali-activated GMK, GWA, and mixture of GWAMK.

Samples	Ra_{eq} (Bq/kg)	H_{ex} (Bq/kg)	\dot{D} (nGy/h)	EDR (mSv/y)
GWA	181.2	0.489	92.9	0.456
GWAMK10	207.0	0.559	104.6	0.513
GWAMK20	202.3	0.546	100.9	0.495
GWAMK30	212.8	0.575	105.1	0.515
GMK	287.9	0.778	131.7	0.646

The results presented in Tables 5 and 6 show that the radium equivalent activity in starting materials ranges from 320.5 Bq/kg to 409.7 Bq/kg, while in the AAM, that range is from 181.2 Bq/kg to 287.9 Bq/kg. In addition, the external radiation hazard index was at its highest value for the starting materials metakaolin (1.107 Bq/kg) and wood ash (1.025 Bq/kg). After alkaline activation of these materials, the value of the external radiation index decreased. This implies a safe application of these AAM and the possibility of their further application in construction sectors. The external gamma radiation absorbed dose rate decreased after alkaline activation of the starting materials and was in the range from 92.9 nGy/h to 131.7 nGy/h.

Based on Janković et al. [42], where Ra_{eq} ranged from 101 to 401 Bq/kg and H_{ex} ranged from 0.28 to 0.88 Bq/kg, it can be seen that investigated alkali-activated form had similar values from 181.2 to 287.9 Bq/kg and from 0.489 to 0.778 Bq/kg, respectively. In case of the external gamma radiation absorbed dose rate and effective dose rate data from the literature [42], the ranges were 47–186 nGy/h and 0.09–1.4 mSv/y, and for alkali-activated samples in this study, those ranges were 92.9–131.7 nGy/h and 0.456–0.646 mSv/y, respectively.

3.2. Structural Analysis

3.2.1. FTIR Analysis

Figure 1a describes the FTIR spectrum of investigated materials MK, WA, and mixture of WAMK (10, 20, and 30%), while Figure 1b shows FTIR spectrum of obtained alkali-activated materials.

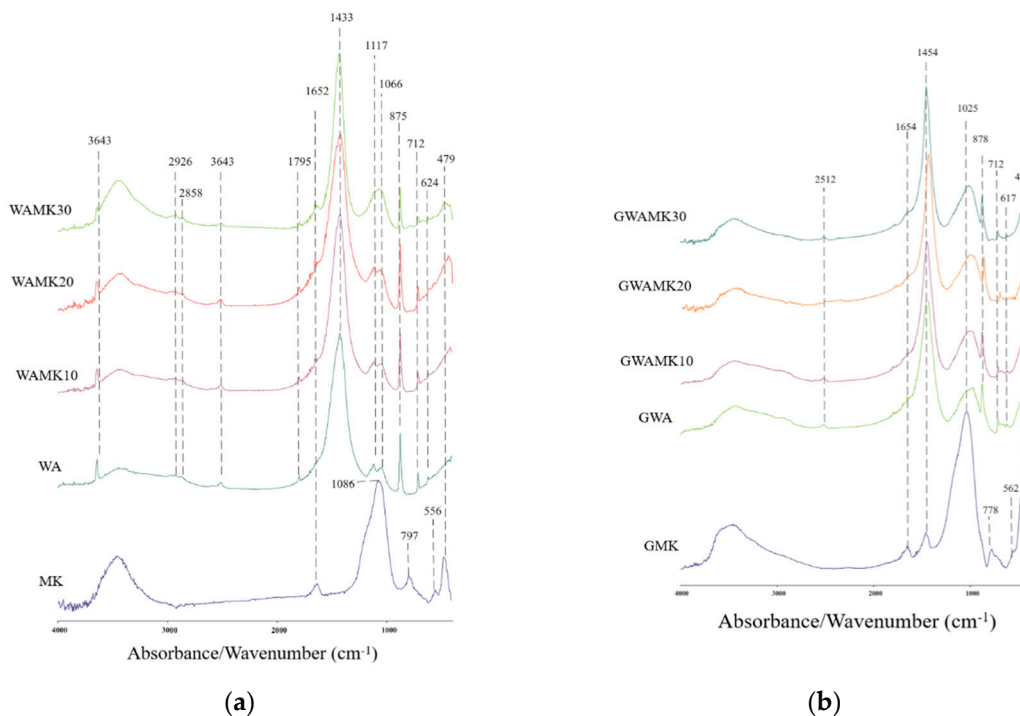


Figure 1. FTIR spectrum of (a) MK, WA, and mixture of WAMK (10, 20, and 30%) and (b) alkali-activated materials.

The presence of two bands in the range of OH-group vibrations was noted in the FTIR spectrum. The band at 3643 cm^{-1} was derived from the regularly distributed group OH in the structure. The wide band $\sim 3450\text{ cm}^{-1}$ was related to a randomly placed hydroxyl group in the structure. The small peak at wave number $\sim 1652\text{ cm}^{-1}$ indicated adsorbed or associated water molecules [43].

Bending vibration of O–Si–O bond in silicate tetrahedron at 479 cm^{-1} was observed in MK and WAMK30, but in other investigated samples this vibration was not observed [43]. For MK, the absorption peaks at approximately 1086 cm^{-1} were associated with asymmetric stretching vibrations of Si–O–Si and Al–O–Si [44]. The weak peak at 1117 cm^{-1} associated with Si–O vibration and peak at 624 cm^{-1} assignable to Mg–O– or K–O bonds were observed in samples of WA and WAMK (10, 20, and 30%). Characteristic Si–O bonding bands at 479 cm^{-1} corresponding to silicon dioxide were also identified, and it is more conspicuous in MK and also visible in WAMK30 [45]. Vibrations associated with symmetric and asymmetric stretches of C–H in the methyl and methylene groups, present in the spectrum of WA and WAMK (10, 20, and 30%) samples, were found at wavelengths 2926 cm^{-1} and 2858 cm^{-1} [46,47], respectively. A peak at 1795 cm^{-1} indicated CO_3^{2-} vibrations, and it was noticeable in sample WA as well as in WAMK (10, 20, and 30%); with the exception of when the share of MK increased, the intensity of the peak decreased [48]. Vibrations of symmetrical stretching of the Si–O–Si bond in MK were observed at 797 cm^{-1} and, as a result of the alkali activation of metakaolin and sample GMK, the bonds shifted towards lower frequencies at 778 cm^{-1} ; in addition, the peak at 712 cm^{-1} observed in other tested samples indicated the presence of Si–O bonds mostly related to quartz [26,49–51]. The FTIR spectra of the wood ash mixture and different proportions of metakaolin showed characteristic bands corresponding to calcite (CaCO_3) at 1433 cm^{-1} , 875 cm^{-1} , and 712 cm^{-1} . After alkaline activation, the band which is characteristic of calcite shifted to the higher wave number with position at 878 cm^{-1} [44]. In all investigated samples, the characteristic stretching asymmetric vibrations C=O and carbonate vibrations at $1430\text{--}1455\text{ cm}^{-1}$ were expected due to the possibility of carbon dioxide formation in highly alkaline wood ash [43]. A vibration at 454 cm^{-1} indicated Si–O bonds in all tested samples, and vibrations at 1025 cm^{-1} were the main characteristic of the alkali-activated materials which represented the Al–O and Si–O bonds [52]. These vibration bands were smaller in relation to the corresponding peak of GMK and moved to a lower wavelength for GWAMK10, GWAMK20, and GWAMK30. This shift has been attributed to polycondensation of alternating Si–O and Al–O bonds establishing the formation of new products that are different from GMK.

3.2.2. XRD Analysis

Figure 2a shows the diffractogram of metakaolin, wood ash, and wood ash/metakaolin (10, 20, and 30%), and Figure 2b shows the diffractogram of alkali-activated products. The mineralogical composition of the present phases was directly determined by X-ray structural analysis.

The obtained data confirmed the presence of several main crystal phases. In the diffractogram of MK, the presence of an amorphous phase, which characterizes some higher background on the diffractogram in the range of $18\text{--}32^\circ 2\theta$, was noticeable, and the presence of kaolinite— $\text{Al}_2(\text{Si}_2\text{O}_5)(\text{OH})_4$, muskovite— $\text{K}(\text{Al}_4\text{Si}_2\text{O}_9(\text{OH})_3$, quartz— SiO_2 , and illite— $\text{KAl}_2(\text{Si}_3\text{Al})\text{O}_{10}(\text{OH})_2$ was also identified. In blends of wood ash and metakaolin, the dominated crystalline phase was calcite— CaCO_3 , followed by smaller amounts of quartz— SiO_2 , larnite, and illite.

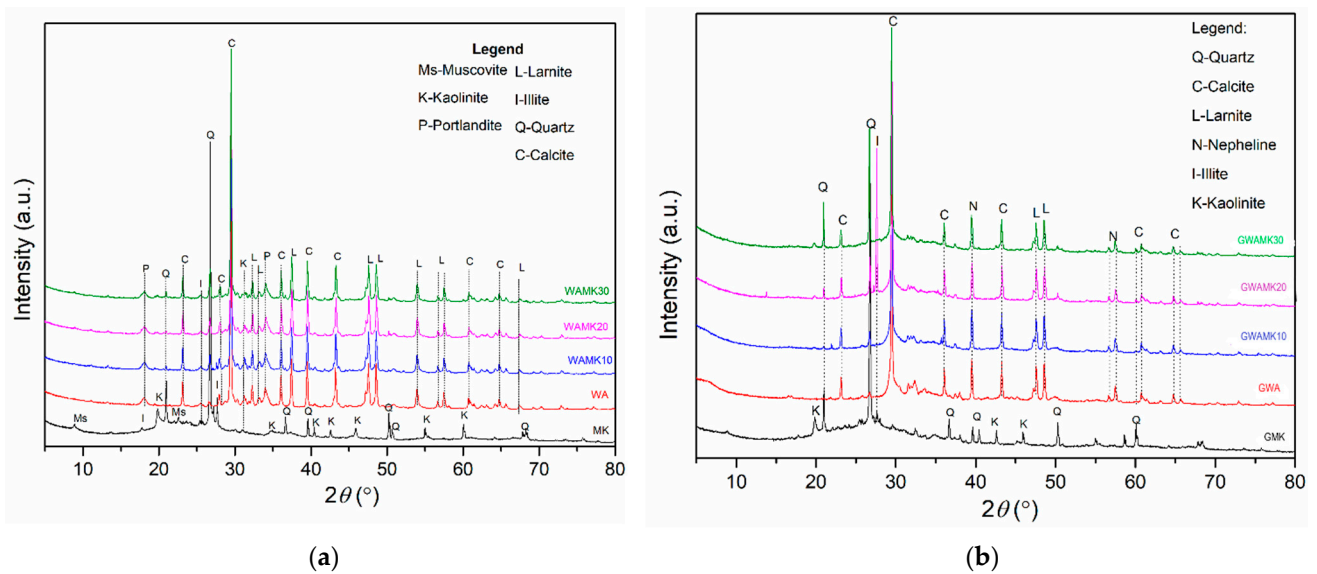


Figure 2. XRD diffractogram of (a) MK, WA, and mixture of WAMK (10, 20, and 30%) and (b) alkali-activated materials.

Materials that occurred from alkali activation of wood ash and blends of wood ash and metakaolin were also analyzed by XRD. In the diffractogram of GMK, the presence of an amorphous phase is observed, which is indicated by a slightly higher background on the diffractogram in the range of approximately $15\text{--}35^\circ 2\theta$, while the crystalline phases were visible only in the GWA sample. The obtained data confirmed that alkali-activated material consisted of calcite— CaCO_3 , quartz— SiO_2 , larnite— $\text{Ca}_2(\text{SiO}_4)$, and illite— $\text{KAl}_2(\text{Si}_3\text{Al})\text{O}_{10}(\text{OH})_2$. In addition, peaks corresponding to nepheline— $\text{NaAlSi}_3\text{O}_8$ were identified. Narrow and well-defined peaks of crystal phase in raw samples, as well as in alkali-activated samples, indicated a proper structural arrangement of identified phases of raw material and alkali-activated materials.

3.2.3. SEM/EDS Analysis

Figure 3 shows SEM micrographs of synthesized alkali-activated samples. All samples showed amorphous gel microstructure and some particles of irregular structure.

Figure 3 shows the morphology of alkali-activated material based on wood ash and blended products of wood ash and metakaolin. There is a noticeable difference between GWA and other activated materials. SEM morphology of GWA (Figure 3a) correspond to amorphous phase with irregularly distributed, agglomerated particles on the surface. In some parts of the sample, the structure is porous, while in others is quite compact. On the surface of individual agglomerated particles, small grains ranging in size from $\sim 0.51\ \mu\text{m}$ to $\sim 1.99\ \mu\text{m}$ are observed. The structure of alkali-activated materials of blend of wood ash and metakaolin differs significantly from structure of alkali-activated pure wood ash (GWA). In GWAMK10 (Figure 3b), agglomerated particles of different sizes are observed. The structure is significantly more porous than the structure of the previous one (GWA). With the addition of MK, an increase in the amorphous phase is noticeable, as a consequence of the formation of the polysialate structure. By adding MK to the wood ash, aluminum is introduced into the system. In GWAMK30 (Figure 3d), the structure is almost compact with the appearance of small grains on the surface of the amorphous, glassy phase.

The elementary composition of analyzed surface of samples: GWA, GWAMK10, GWAMK20, and GWAMK30 is shown in Table 7.

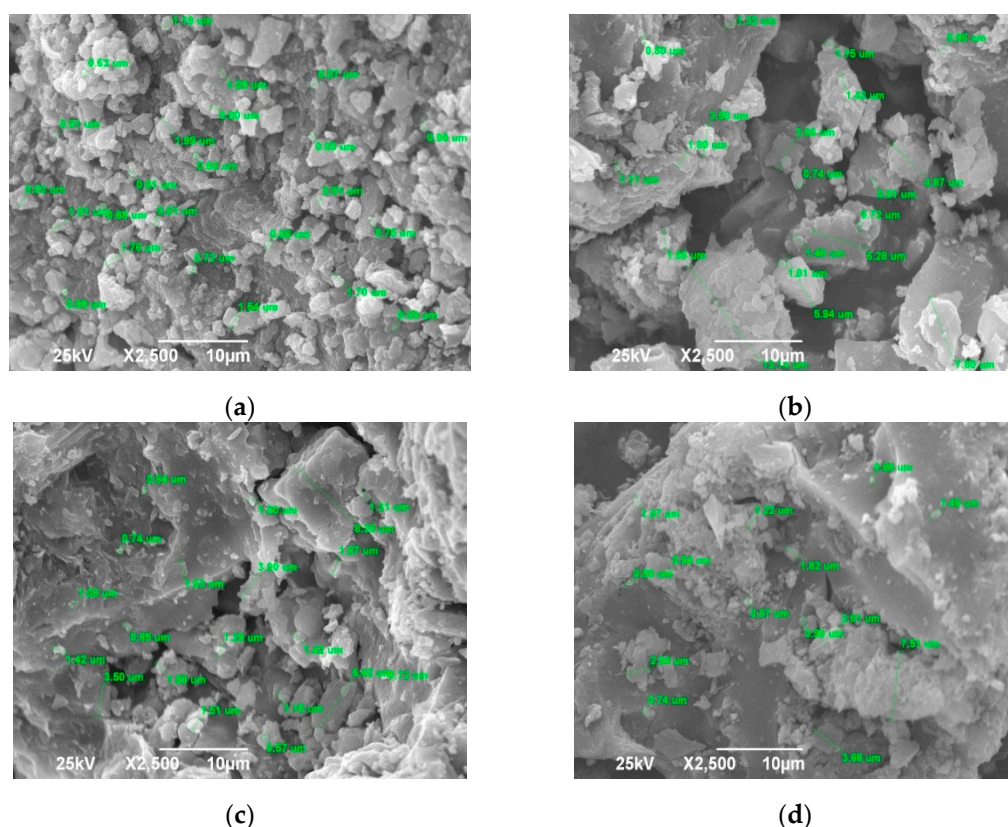


Figure 3. SEM micrographs alkali-activated materials (a) GWA; (b) GWAMK10; (c) GWAMK20; and (d) GWAMK30.

Table 7. The elementary composition (Wt%) of analyzed surface of alkali-activated materials: GWA, GWAMK10, GWAMK20, and GWAMK30.

Element	GWA	GWAMK10	GWAMK20	GWAMK30
C	18.0	26.3	15.1	30.2
O	41.9	40.1	38.5	40.0
Na	7.18	6.61	4.78	4.80
Mg	0.55	0.82	0.47	0.45
Al	/	0.89	1.74	1.43
Si	5.12	6.70	7.06	6.91
K	5.44	3.46	4.10	2.73
Ca	17.5	12.3	24.4	13.5
Mn	0.73	0.41	0.43	/
Cu	1.80	1.32	1.73	/
Zn	1.73	1.04	1.69	/

By semiquantitative analysis of the investigated area of alkali-activated samples, i.e., energy-dispersive X-ray spectroscopy (EDS) analysis, the presence of C, O, Na, Mg, Si, K, Ca, Cu, Mn, Zn, and Mg was determined. The content of C and Ca (18% and 17.5%) was approximately the same, and the content of K and Si (~5%) was the same in GWA; thus, it can be concluded that this sample had a high value of Ca. The absence of Al in GWA indicated that there is no possibility to create Al–O and Al–O–Si bonds in the alkali-activated material based on pure wood ash, which means that the consolidation and formation of the gel structure of the material occurred only through Si–O–Si bonds. Aluminum was not found in alkali-activated pure wood ash. This is why it is necessary to add aluminosilicate material to the WA in order to create an Al–Si–O network. However, the presence of calcium affected the formation of calcium hydroxide. When alkali activator NaOH/Na₂SiO₃ was added to wood ash, the reaction released Ca²⁺, OH[−], and a heat. The mixture reached

higher pH than in the starting solutions. Eventually, the system became saturated, and $\text{Ca}(\text{OH})_2$ started to crystallize along with calcium silicate hydrate. The new materials consisted of a mass of crystals interlocked with each other, with all the other substances present. Carbon dioxide from the air reacted with the calcium hydroxide in materials to form calcium carbonate. This reaction was a slow and continuous progression from the outer surface inward. Carbonation increased the mechanical strength of materials.

4. Conclusions

On the basis of the obtained results presented in this paper, it can be concluded that metakaolin and wood ash are suitable for obtaining alkali-activated materials with satisfactory radiological and structural characteristics. The values obtained through radiological analysis in this study and the calculated maximum $R_{a_{eq}}$ values for alkali-activated samples of wood ash, metakaolin, and their blends are lower than the recommended maximum level (370 Bq/kg), providing an excess annual effective dose of less than 1 mSv; from this point of view, the tested materials do not pose a significant radiation hazard and their use is considered safe for the population. Results of activity concentration measurements in alkali-activated materials, which are 30–50% lower than activity concentration of corresponding raw materials, allow for the conclusion that alkali-activated materials from that aspect can be considered as a potentially safe application in building construction. The values of the external radiation hazard index (Hex) are in the range from 0.489 Bq/kg to 0.788 Bq/kg for alkali-activated materials and are lower compared with the raw materials used for their production. Since Hex values are below unity, it means that the radiation hazard of alkali-activated materials is kept to an insignificant level.

Structural characterization of synthesized materials was performed by using XRD, FTIR, and SEM/EDS techniques. FTIR analysis of WAMK10, WAMK20, and WAMK30 shows characteristic bands corresponding to calcite. The main characteristic of the alkali-activated materials is observed at 1025 cm^{-1} , which represents the Al–O and stretching Si–O bonds, and the peak at 454 cm^{-1} indicates bending Si–O bonds. XRD analysis showed that MK consists predominantly of kaolinite and quartz, with minor admixtures of muscovite and illite, while in WAMK10, WAMK20, and WAMK30, the predominant crystalline phase is calcite. All alkali-activated samples mainly consist of calcite, quartz, larnite, and illite but also contain a crystalline phase corresponding to nepheline. SEM analysis shows that alkali-activated materials are porous, and with the increase of the ratio of MK, it becomes quite compact. EDS analysis of the investigated area of alkali-activated samples shows the presence of C, O, Na, Mg, Si, K, Ca, Cu, Mn, Zn, and Mg. It is a semiquantitative analysis that can only serve as a guide in interpreting the results.

Author Contributions: Conceptualization, N.N.M.N., L.M.K. and S.S.N.; methodology, N.N.M.N.; validation, I.S.V. and L.M.K.; formal analysis, M.M.M. and A.B.K.; investigation, N.N.M.N.; data curation, A.B.K. and S.S.N.; writing—original draft preparation, N.N.M.N. and L.M.K.; writing—review and editing, S.S.N., K.V.T., M.M.M. and I.S.V.; visualization, K.V.T.; supervision, L.M.K. All authors have read and agreed to the published version of the manuscript.

Funding: This work was financially supported by the Ministry of Education, Science and Technological Development of Republic of Serbia on the research program, record number: 451-03-68/2022-14/200017 grant No. 1702202 and grant No. 1002202 Vinča Institute of Nuclear Sciences, National Institute of the Republic of Serbia, University of Belgrade, Serbia.

Informed Consent Statement: Not applicable.

Data Availability Statement: Not applicable.

Acknowledgments: Our special thanks go to Vladimir B. Pavlović, Full Professor and Principal Research Fellow, for her support in providing SEM/EDS analysis, and Bratislav Ž. Todorović, Full Professor, for his support in providing FTIR analysis.

Conflicts of Interest: The authors declare no conflict of interest.

References

1. ReferencesKhale, D.; Chaudhary, R. Mechanism of geopolymerization and factors influencing its development: A review. *J. Mater. Sci.* **2007**, *42*, 729–746.
2. Abdulkareem, O.A.; Ramli, M.; Matthews, J.C. Production of geopolymer mortar system containing high calcium biomass wood ash as a partial substitution to fly ash: An early age evaluation. *Compos. B Eng.* **2019**, *174*, 106941. [[CrossRef](#)]
3. Rocha, T.S.; Dias, D.P.; França, F.C.C.; Guerra, R.R.S.; Marques, L.R.C.O. Metakaolin-based geopolymer mortars with different alkaline activators (Na⁺ and K⁺). *Constr. Build. Mater.* **2018**, *178*, 453–461. [[CrossRef](#)]
4. Leong, H.Y.; Ong, D.E.L.; Sanjayan, J.G.; Nazari, A. Strength Development of Soil-Fly Ash Geopolymer: Assessment of Soil, Fly Ash, Alkali Activators, and Water. *J. Mater. Civ. Eng.* **2018**, *30*, 04018171. [[CrossRef](#)]
5. Buchwald, A.; Schulz, M. Alkali-activated binders by use of industrial by-products. *Cem. Concr. Res.* **2005**, *35*, 968–973. [[CrossRef](#)]
6. Pacheco-Torgal, F.; Castro-Gomes, J.; Jalali, S. Alkali-activated binders: A review. Part 2. About materials and binders manufacture. *Constr. Build. Mater.* **2008**, *22*, 1315–1322. [[CrossRef](#)]
7. Wang, Y.-S.; Alrefaei, Y.; Dai, J.-G. Silico-Aluminophosphate and Alkali-Aluminosilicate Geopolymers: A Comparative Review. *Front. Mater.* **2019**, *6*, 106. [[CrossRef](#)]
8. Nenadović, S.S.; Kljajević, L.M.; Nešić, M.A.; Petković, M.Ž.; Trivunac, K.V.; Pavlović, V.B. Structure analysis of geopolymers synthesized from clay originated from Serbia. *Environ. Earth Sci.* **2017**, *76*, 79. [[CrossRef](#)]
9. Zhang, Z.; Provis, J.L.; Reid, A.; Wang, H. Geopolymer foam concrete: An emerging material for sustainable construction. *Constr. Build. Mater.* **2014**, *56*, 113–127. [[CrossRef](#)]
10. Ameri, F.; Shoaie, P.; Zareei, S.A.; Behforouz, B. Geopolymers vs. alkali-activated materials (AAMs): A comparative study on durability, microstructure, and resistance to elevated temperatures of lightweight mortars. *Constr. Build. Mater.* **2019**, *222*, 49–63. [[CrossRef](#)]
11. Mladenović, N.; Kljajević, L.J.; Nenadović, S.; Ivanović, M.; Čalija, B.; Gulicovski, J.; Trivunac, K. The applications of new inorganic polymer for adsorption cadmium from waste water. *J. Inorg. Organomet. Polym. Mater.* **2020**, *30*, 554–563. [[CrossRef](#)]
12. Rakhimov, N.R.; Rakhimov, R.Z. Reaction products, structure and properties of alkali-activated metakaolin cements incorporated with supplementary materials—a review. *J. Mater. Res. Technol.* **2019**, *8*, 1522–1531. [[CrossRef](#)]
13. Glavonjić, B. Consumption of Wood Fuels in Households in Serbia—Present State and Possible Contribution to the Climate Change Mitigation. *Therm. Sci.* **2011**, *15*, 571–585. [[CrossRef](#)]
14. Elinwa, A.U.; Mahmood, Y.A. Ash from timber waste as cement replacement material. *Cem. Concr. Compos.* **2002**, *24*, 219–222. [[CrossRef](#)]
15. Wang, S.; Miller, A.; Llamazos, E.; Fonseca, F.; Baxter, L. Biomass fly ash in concrete: Mixture proportioning and mechanical properties. *Fuel* **2008**, *87*, 365–371. [[CrossRef](#)]
16. Da Luz Garcia, M.; Sousa-Coutinho, J. Strength and durability of cement with forest waste bottom ash. *Constr. Build. Mater.* **2013**, *41*, 897–910. [[CrossRef](#)]
17. Vaičiukynienė, D.; Michalik, B.; Bonczyk, M.; Vaičiukynas, V.; Kantautas, A.; Krulikauskaitė, J. Zeolitized bottom ashes from biomass combustion as cement replacing components. *Constr. Build. Mater.* **2018**, *168*, 988–994. [[CrossRef](#)]
18. Teixeira, E.R.; Camões, A.; Branco, F.G. Valorisation of wood fly ash on concrete. *Resour. Conserv. Recycl.* **2019**, *145*, 292–310. [[CrossRef](#)]
19. Pokorný, J.; Zemanová, L.; Pavlíková, M.; Pavlík, Z. Properties of Alkali-Activated Composites Containing Biomass Ash. *AIP Conf. Proc.* **2019**, *2170*, 020016.
20. Vassilev, S.V.; Baxter, D.; Andersen, L.K.; Vassileva, C.G. An overview of the chemical composition of biomass. *Fuel* **2010**, *89*, 913–933. [[CrossRef](#)]
21. Ban, C.C.; Ramli, M. The implementation of wood waste ash as a partial cement replacement material in the production of structural grade concrete and mortar: An overview. *Resour. Conserv. Recycl.* **2011**, *55*, 669–685.
22. Ban, C.C.; Ramli, M. Properties of high calcium wood ash and densified silica fume blended cement. *Int. J. Phys. Sci.* **2011**, *6*, 6596–6606.
23. Ban, C.C.; Ramli, M. Characterisation of High Calcium Wood Ash for Use as a Constituent in Wood Ash-Silica Fume Ternary Blended Cement. *Adv. Mat. Res.* **2012**, *346*, 3–11. [[CrossRef](#)]
24. Temuujin, J.; Minjigmaa, A.; Davaabal, B.; Bayarzul, U.; Ankhtuya, A.; Jadambaa Ts MacKenzie, K.J.D. Utilization of radioactive high-calcium Mongolian fly ash for the preparation of alkali-activated geopolymers for safe use as construction materials. *Ceram. Int.* **2014**, *40*, 16475–16483. [[CrossRef](#)]
25. Janković, B.Ž.; Janković, M.M.; Marinović-Cincović, M.M.; Todorović, D.J.; Sarap, N.B. Thermal analysis testing and natural radioactivity characterization of kaolin as building material. *J. Therm. Anal. Calorim.* **2018**, *133*, 481–487. [[CrossRef](#)]
26. Ivanović, M.; Kljajević, L.J.; Nenadović, M.; Bundaleski, N.; Vukanac, I.; Todorović, B.; Nenadović, S. Physicochemical and radiological characterization of kaolin and its polymerization products. *Mater. Construcción* **2018**, *68*, e155. [[CrossRef](#)]
27. Kljajević, L.M.; Melichova, Z.; Stojmenović, M.D.; Todorović, B.Ž.; Pavlović, V.B.; Čitaković, N.M.; Nenadović, S.S. Structural and electrical properties of geopolymer materials based on different precursors (kaolin, bentonite and diatomite). *Maced. J. Chem. Chem. Eng.* **2019**, *38*, 283–292. [[CrossRef](#)]
28. International Atomic Energy Agency. *Measurement of Radionuclides in Food and the Environment, A Guide Book*; Technical Reports Series No. 295; IAEA: Vienna, Austria, 1989.

29. MBSS 2, Cert. No. 9031-OL-032/05; Radioactive Standard. CMI (Czech Metrological Institute): Prague, Czech Republic, 2005.
30. Beretka, J.; Mathew, P.J. Natural radioactivity of Australian building materials, industrial wastes and by-products. *Health Phys.* **1985**, *48*, 87–95. [[CrossRef](#)] [[PubMed](#)]
31. Janković Mandić, L.J.; Dragović, S. Assessment of terrestrial gamma exposure to the population of Belgrade (Serbia). *Radiat. Prot. Dosim.* **2010**, *140*, 369–377. [[CrossRef](#)] [[PubMed](#)]
32. UNSCEAR, United Nations Scientific Committee on the Effects of Atomic Radiation. *Sources, Effects and Risks of Ionizing Radiation. Report to the General Assembly with Annex A: Exposures from Natural Sources of Radiation*; United Nations: New York, NY, USA, 1993.
33. Madruga, M.J.; Miró, C.; Reis, M.; Silva, L. Radiation exposure from natural radionuclides in building materials. *Radiat. Prot. Dosim.* **2019**, *185*, 49–57. [[CrossRef](#)] [[PubMed](#)]
34. Rigaku. *PDXL Integrated X-Ray Powder Diffraction Software*; Version 2.8.4.0; Rigaku: Tokyo, Japan, 2011.
35. International Crystallographical Data Base (ICDD). Available online: <https://www.icdd.com/> (accessed on 17 August 2022).
36. Ilić, S.B.; Golubović, T.D.; Pajić, N.D.; Djurašević, M.M.; Kandić, A.B. Analysing radionuclide content in soil samples and radiological risks in the clayey material surrounding of the „Zbegovi“ deposit, Donje Crniljevo, Serbia. *Nucl. Technol. Radiat. Prot.* **2020**, *35*, 154–164. [[CrossRef](#)]
37. Šešlak, B.; Ujić, P.; Vukanac, I.; Kandić, A.; Đurašević, M.; Čeliković, I.; Milošević, Z. Content of ^{137}Cs and ^{40}K in wood ash. *Ecologica* **2015**, *22*, 605–608.
38. Ladygienė, R.; Orentienė, A.; Pilkytė, L.; Skripkienė, A.; Žukauskaitė, V.; Kievinas, R. Radiological investigation of wood used for combustion. *Ekologija* **2010**, *56*, 87–93. [[CrossRef](#)]
39. Hus, M.; Košutić, K.; Lulić, S. Radioaktivnost Drva i Okoliša. V. simpozij HDZZ, Stubičke Toplice. 2003, pp. 329–334. Available online: https://inis.iaea.org/collection/NCLCollectionStore/_Public/34/051/34051978.pdf (accessed on 2 August 2022).
40. Marčiulionienė, D.; Lukšienė, B.; Kiponas, D.; Maksimov, G.; Darginavičienė, J.; Gavelienė, V. Effects of ^{137}Cs and ^{90}Sr on the plant *Lepidium sativum* L. growth peculiarities. *Ekologija* **2007**, *53*, 65–70.
41. Stoulos, S.; Ioannidou, A.; Vagena, E.; Koseoglou, P.; Manolopoulou, M. Post-Chernobyl ^{137}Cs in the atmosphere of Thessaloniki: A consequence of the financial crisis in Greece. *J. Environ. Radioact.* **2014**, *128*, 68–74. [[CrossRef](#)]
42. Janković, M.M.; Todorović, D.J.; Nikolić, J.D. Analysis of natural radionuclides in coal, slag and ash in coal-fired power plants in Serbia. *J. Min. Metall. B Metall.* **2011**, *47*, 149–155. [[CrossRef](#)]
43. Li, F.; Wu, W.; Li, R.; Fu, X. Adsorption of phosphate by acid-modified fly ash and palygorskite in aqueous solution: Experimental and modeling. *Appl. Clay Sci.* **2016**, *132–133*, 343–352. [[CrossRef](#)]
44. Lin, W.Y.; Prabhakar, A.K.; Mohan, B.C.; Wang, C.-H. A factorial experimental analysis of using wood fly ash as an alkaline activator along with coal fly ash for production of geopolymer cementitious hybrids. *Sci. Total Environ.* **2020**, *718*, 135289. [[CrossRef](#)]
45. Ngueyep, M.; Fotseu, L.L.C.; Christian, M.; Elie, C.K. Valorization of Wood Ashes as Partial Replacement of Portland Cement: Mechanical Performance and Durability. *Eur. J. Sci. Res.* **2019**, *151*, 468–478.
46. Poletto, M.; Zattera, A.J.; Santana, R.M.C. Structural differences between wood species: Evidence from chemical composition, FTIR spectroscopy, and thermogravimetric analysis. *J. Appl. Polym. Sci.* **2012**, *126*, E337–E344. [[CrossRef](#)]
47. Kubovský, I.; Kačíková, D.; Kačík, F. Structural Changes of Oak Wood Main Components Caused by Thermal Modification. *Polymers* **2020**, *12*, 485. [[CrossRef](#)] [[PubMed](#)]
48. Ylmén, R.; Jäglid, U. Carbonation of Portland Cement Studied by Diffuse Reflection Fourier Transform Infrared Spectroscopy. *Int. J. Concr. Struct. Mater.* **2013**, *7*, 119–125. [[CrossRef](#)]
49. Kalemkiewicz, J.; Galas, D.; Sitarz-Palczak, E. The Physicochemical Properties and Composition of Biomass Ash and Evaluating Directions of its Applications. *Pol. J. Environ. Stud.* **2018**, *27*, 2593–2603. [[CrossRef](#)]
50. Tian, Q.; Sasaki, K. Application of fly ash-based geopolymer for removal of cesium, strontium and arsenate from aqueous solutions: Kinetic, equilibrium and mechanism analysis. *Water Sci. Technol.* **2019**, *79*, 2116–2125. [[CrossRef](#)]
51. Siyal, A.A.; Shamsuddin, M.R.; Rabat, N.E.; Zulfiqar, M.; Man, Z.; Low, A. Fly ash based geopolymer for the adsorption of anionic surfactant from aqueous solution. *J. Clean. Prod.* **2019**, *229*, 232–243. [[CrossRef](#)]
52. Nasab, G.M.; Golestanifard, F.; MacKenzie, K.J.D. The effect of the $\text{SiO}_2/\text{Na}_2\text{O}$ ratio in the structural modification of metakaolin-based geopolymers studied by XRD, FTIR and MAS-NMR. *J. Ceram. Sci. Technol.* **2014**, *5*, 185–192.